Volume 5 | Number 3 | May 2018 | Pages 311–580

Materials Horizons

rsc.li/materials-horizons

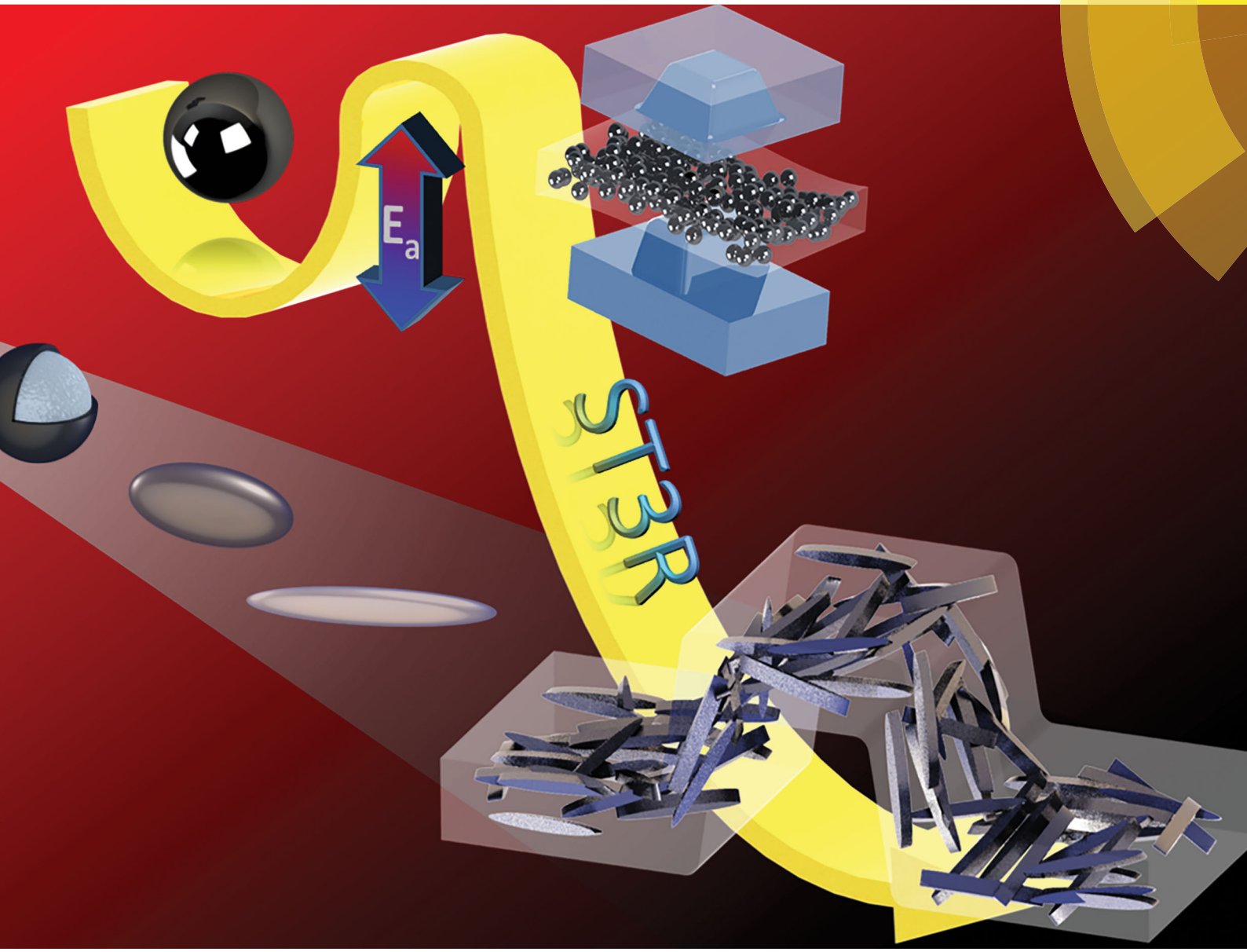

ISSN 2051-6347

ROYAL SOCIETY OF CHEMISTRY

COMMUNICATION

Michael D. Bartlett, Martin M. Thuo *et al.*

Mechanically triggered composite stiffness tuning through thermodynamic relaxation (ST3R)

Materials Horizons

COMMUNICATION

View Article Online
View Journal | View Issue

Cite this: *Mater. Horiz.*, 2018, 5, 416

Received 10th January 2018,
Accepted 23rd January 2018

DOI: 10.1039/c8mh00032h

rsc.li/materials-horizons

Mechanically triggered composite stiffness tuning through thermodynamic relaxation (ST3R)†

Boyce S. Chang, Ravi Tutika, Joel Cutinho, Stephanie Oyola-Reynoso, Jiahao Chen, Michael D. Bartlett * and Martin M. Thuo *

Recent developments in smart responsive composites have utilized various stimuli including heat, light, solvents, electricity, and magnetic fields to induce a change in material properties. Here, we report a thermodynamically driven mechanically responsive composite, exploiting irreversible phase-transformation (relaxation) of metastable undercooled liquid metal core shell particle fillers. Thermal and mechanical analysis reveals that as the composite is deformed, the particles transform from individual liquid droplets to a solid metal network, resulting in a 300% increase in Young's modulus. In contrast to previous phase change materials, this dramatic change in stiffness occurs autonomously under deformation, is insensitive to environmental conditions, and does not require external energy sources such as heat, light, or electricity. We demonstrate the utility of this approach by transforming a flat, flexible composite strip into a rigid, 3D structure that is capable of supporting 50× its own weight. The ability for shape change and reconfiguration are further highlighted, indicating potential for multiple pathways to trigger or tune composite stiffness.

Conceptual insights

This article highlights a non-traditional approach to fabricating autonomously stiffening materials. Instead of relying on stress induced chemical reactions, we exploit the metastability of undercooled liquid metal particles. Relaxation of the metastable particles (solidification) is triggered by mechanical stresses. Coupling such a trigger with thermodynamic instability has not been employed in the design of smart composites due to the complexity of synthesizing metastable materials. Here we overcome this constraint with a simple fabrication approach and demonstrate a unique combination of metastability and mechanical activation, which introduces important new concepts for stimuli-responsive materials.

Interest in synthetic composite materials has garnered significant attention largely due to their high specific properties, tunable functionalities, and potential to incorporate advanced responsive behaviors.[1] Recent advances have largely focused on stimuli-responsive composites,[2] which exhibit tunable properties when subjected to a specified trigger.[3–7] Such materials have been applied as sensors, actuators, and platforms for multifunctional devices.[8–17] Mechanically reconfigurable parts are especially critical in soft robotics and analogous functional devices, whereby adaptive components are essential for controlled locomotion, actuation, stiffness tuning, and as deployable components.[18–20] In particular, initially soft materials that can dramatically increase in rigidity and be programmed into desired shapes can be utilized in fields ranging from soft and bio-inspired robotics to reconfigurable and wearable electronics. Several forms of activation have been applied in responsive composites, and common examples include temperature,[21–24] electromagnetic radiation,[25] as well as electric and magnetic fields.[26–28] Mechanically triggered response, although less frequently used, can offer important functionalities such as mechanically actuated sensors, self-healing and self-strengthening. Interestingly, bistable and interleaved structures have been applied to produce responsive composites by mechanical and thermal activation.[29–32] Mechanical energy has been used to rupture particulate fillers leading to self-healing and dissipation of stress to inhibit crack propagation.[33,34] More recently, mechanochemically activated polymers that display self-strengthening behaviour when subjected to shear forces have been developed.[35–40] In general, mechanically induced stiffening/strengthening is achieved by triggering polymerization or cross-linking of the polymer chains. The application of chemical reactions, however, suffers from diffusion and reaction kinetics limitations, and can potentially fail under non-ideal conditions (*e.g.* moiety degradation or presence of adventitious inhibitor).

Coupling a trigger like mechanical stress with a thermodynamic response (*e.g.* phase transformation[21,22,41–43]) has not been widely deployed in the design of stimuli-responsive composites.

Department of Materials Science and Engineering, Iowa State University, 2240 Hoover Hall, 528 Bissell Rd, Ames, IA, USA. E-mail: mthuo@iastate.edu, mbartlet@iastate.edu

† Electronic supplementary information (ESI) available. See DOI: 10.1039/c8mh00032h

The limited expansion of trigger mechanisms into thermodynamic processes is in part due to the complexity of synthesizing a composite material whose thermodynamic potential dictates a transient equilibrium state, yet with a large enough activation barrier or significantly slow kinetics to remain stable prior to activation. A potential approach to this type of coupled stimuli-response is to embed a metastable material such as an undercooled liquid into a matrix. Relaxation of the metastable material leads to significant changes in properties of the composite, especially where such change can be externally triggered. Felicitous choice of such metastable filler-matrix pairs, expands the array of stimuli, responses, or properties that can be accessed. Here we demonstrate a thermodynamically controlled self-stiffening composite. This approach entails incorporating thermodynamically frustrated (metastable) undercooled liquid metal core–shell (ULMCS) particles into an elastomer matrix followed by mechanically triggered shape change with concomitant solidification (schematically illustrated in Fig. 1a). The addition of metal fillers increases the density of the composite, however, metal composites have been implemented due to their high strength and potentially responsive properties.[44,45] The ULMCS particles (Fig. 1b) are obtained by frustrating solidification of a molten metal, through a core–shell (oxide/liquid metal) particle architecture (Fig. 1a), well below its melting temperature (T_m).[46] Upon mechanical rupture of the particle shell, the liquid flows, fuses, and rapidly solidifies (Fig. 1b to c), reverting to the stiffness of the bulk metal. When this transition occurs in an elastomeric matrix, a transformation from a soft flexible composite to a rigid, load-bearing material occurs (Fig. 1d to e). Through a combination of characterization techniques, we herein show that: (1) metastable ULMCS particles can be incorporated into a polymer matrix without triggering solidification during fabrication (Fig. 1a and d), (2) upon applying mechanical stress to the composite, shape change and solidification of the ULMCS particles result in a stiffened composite (Fig. 1a, c and e), and (3) solidification of the metal locks the matrix in position, leading to shape change. This Stiffness tuning through thermodynamics relaxation (abbreviated ST3R for clarity and brevity) approach enables the composites to support 50 times its own weight after compressive shaping with a mold (Fig. 1e). Such a large change in stiffness is not observed in the case of a pure polymer matrix or pure solid metal, hence, unique to the ST3R composite (Fig. 2). This irreversible mechanically induced phase transformation of metastable particles does not require external heat sources or electrical stimulation, providing an autonomous approach to self-stiffening when a material is subjected to mechanical stress during load-bearing applications.

Thermodynamics in design of ST3R composites. Metastable ULMCS particles of field's metal (FM, $E \approx 9.25 \times 10^3$ MPa[47]) and stable liquid particles of eutectic gallium–indium (EGaIn) are synthesized using the SLICE method, a simple and low cost method of creating liquid metal core shell (LMCS) particles.[48] This modified emulsification method involves shearing liquid metals in a solution of a chelating agent to produce spherical core–shell particles.[46,48] The presence of a thin passivating oxide,[49] stabilized by an organic ligand, on the surface of the liquid particles renders them stable and incapable of coalescence.[48] Undercooling is achieved by trapping the metal in a disordered liquid state (high entropy) while simultaneously eliminating heterogeneous nucleation sites. This architecture creates a thermal (E_a, state 1, Fig. 1f) and kinetic barrier to solidification of the liquid metal (state 1, Fig. 1f). Sufficient mechanical deformation fractures the thin oxide shell and introduces heterogeneous nucleation sites, hence sufficient activation to overcome the E_a (Fig. 1f) and initiate solidification and relaxation to the global energy minima – the solid state (state 2, Fig. 1f). This transition from state 1 to 2 is irreversible (2nd law of thermodynamics). In state 2, the material is now

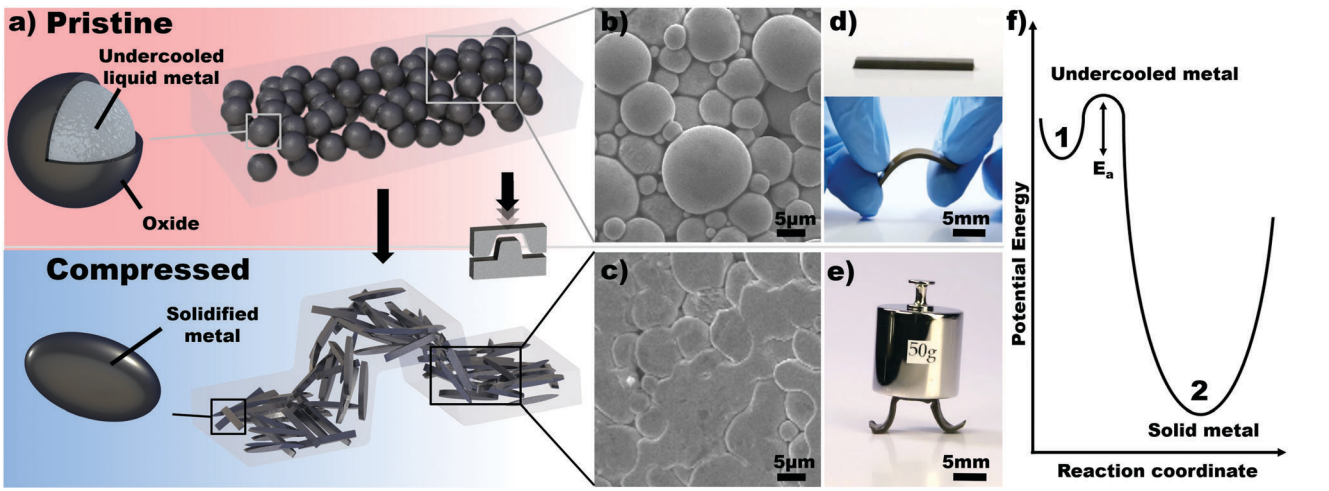

Fig. 1 (a) Schematic illustration of stiffness tuning through thermodynamic relaxation (ST3R) in a composite through solidification of the undercooled metal particle fillers with concomitant reconfiguration of the material. (b) Scanning electron micrograph of field's metal (FM) undercooled metal particles. (c) Fused and solidified particles after mechanical rupture of the oxide shell. (d) A sample of flexible undercooled FM particles loaded ST3R composite. (e) Mechanically reconfigured composite, capable of holding 50× its own weight. (f) Energy landscape of the undercooled liquid metal relative to its solid counterpart.

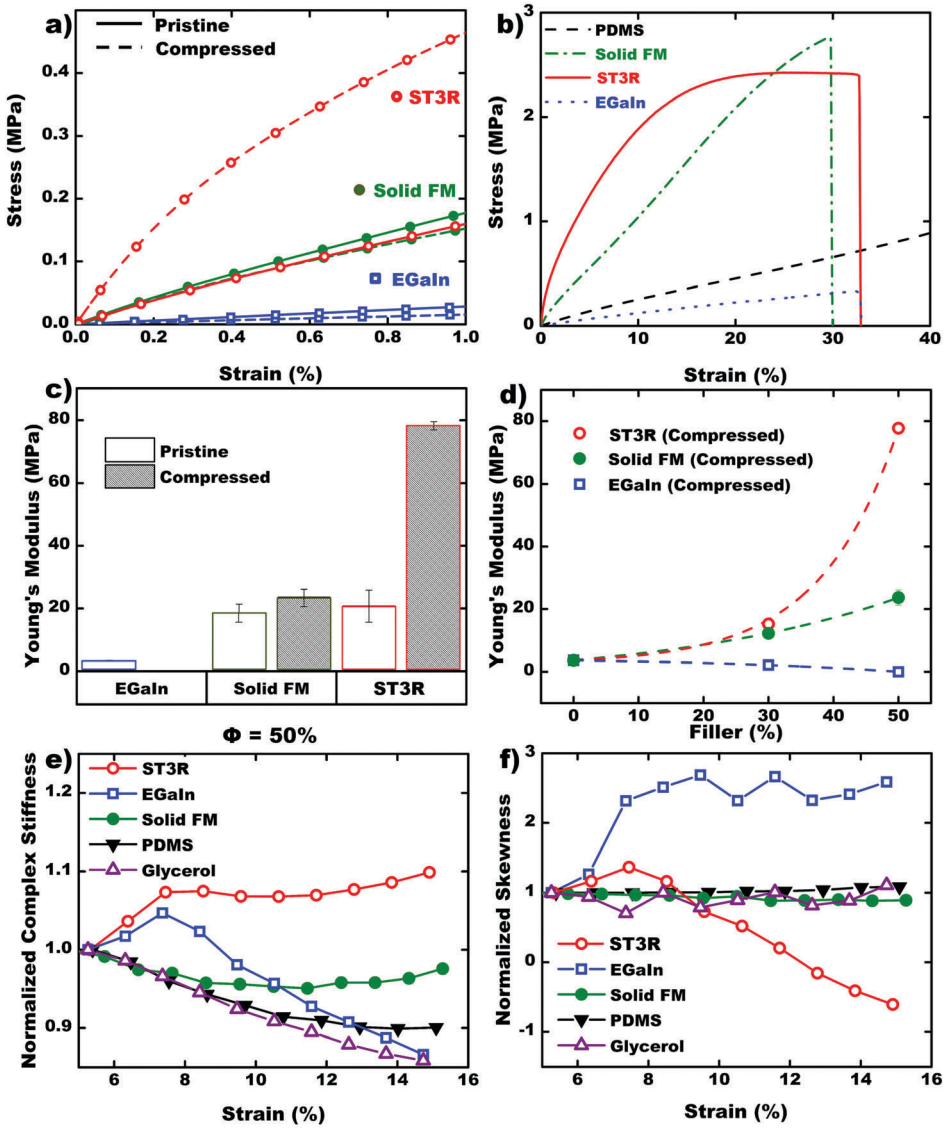

Fig. 2 (a) Stress–strain curve of pristine and pre-compressed ϕ = 50% composites at low strain (1%). (b) Stress–strain curve of pre-compressed ϕ = 50% composites (For EGaIn ϕ = 30% data is presented as the 50% samples fractured upon compression). (c) Comparison between the Young's modulus of pristine and compressed ϕ = 50% composite. (d) Young's modulus (0.2% strain) of composites after compression with increasing ϕ. (e) Normalized complex stiffness with increasing cyclic strain of ϕ = 22%. composites. (f) Normalized skewness in the distribution of complex stiffness.

comparable to a conventional metal–elastomer composite albeit with non-spherical fillers.[21,22,47] Since the SLICE technique produces particles with varying sizes, the total number of metal atoms, hence the thermodynamic potential, in each particle of a given size is different. A Gaussian distribution in particle size (polydispersity) is expected leading to a Maxwell–Boltzmann type energy distribution (eqn (1)), where energy state degeneracy is unrestricted and depends on particle size.

$$\frac{N_i}{N} = \frac{g_i e^{-\beta' \varepsilon_i}}{Z} \quad (1)$$

where N_i is number of particles of a given size (energy), N is total number of particles, z is the normalization constant while ε_i is the energy of a particle of a given energy (size) in energy state (size bin) g_i, β' is the temperature-dependent Lagrangian multiplier.

Response of ST3R composites upon mechanical activation is, therefore, expected to follow a similar distribution, albeit with a drift towards higher modulus as low E_a particles transition under lower strain leading to a stiffer dispersed phase. This transition leads to a skewed Maxwell–Boltzmann distribution in the energy states of the remaining undercooled particles. This understanding of thermodynamic potential distribution implies that ST3R composites mechanically change in line with a thermodynamic potential landscape that is governed by the distribution in the energy states of the undercooled particle fillers that are, in part, dictated by their size and propensity for the shell to yield under mechanical stress.

Preparation of ST3R composites. Differential scanning calorimetry (DSC, Fig. S1, ESI†) and microscopic imaging (SEM, Fig. 1b) of the particles confirm the liquid core nature of the synthesized particles. DSC demonstrates that >90% of the freezing event is centered at 7 °C (T_m = 62 °C) (Fig. S1, ESI†). These particles are incorporated into a silicone elastomer matrix (Dow Corning Sylgard® 184, 10 : 1 Base : catalyst ratio. E = 3.65 MPa (measured)) to form a field's metal ULMCS particle–elastomer composite (ST3R composite). Details regarding ST3R and other composite fabrication procedures are provided in the Experimental section.

Characterization of the ST3R composite. To investigate mechanically triggered phase-change driven stiffness enhancement of the composites, we performed tensile tests on pristine and pre-compressed samples (details on the compression procedure are provided in the ESI,† Fig. S2). In Fig. 2a and b, we show tensile stress–strain curves for pristine (solid line) and pre-compressed (dashed line) composites at filler volume fraction, ϕ = 50%, comparing ST3R with two similarly prepared control samples of ambient liquid metal (eutectic gallium indium, EGaIn) and solid FM particles of comparable dimensions. We observe that the pre-compressed ST3R composite shows a significant increase in initial stiffness (Fig. 2a), while both EGaIn and solid FM particles samples show an insignificant change due to compression. We infer that the dramatic increase in stiffness is due to solidification of ULMCS particles, that is; transformation of the initially liquid particles into a solid metal, likely with concomitant formation of an interconnected network due to inter-particle fusion. ST3R composite in fact becomes electrically conductive after compression. The material exhibits a 300% increase in Young's modulus (~80 MPa), significant transition from a flexible low modulus as-prepared parent (Fig. 2c). We expect latent heat of solidification to be released into the matrix, however, estimated dissipation time based on Fourier's law indicates that the change in temperature would be largely unnoticeable. In contrast, the EGaIn sample fractured upon compression while solid FM composites show a statistically insignificant increase in stiffness. To confirm differences in mechanical properties of the compressed samples, we subject the materials to high stresses, expecting that shape change and network formation will differentiate compressed ST3R composite from solid FM samples (Fig. 2b). Besides the larger (300%) initial stiffness for ST3R, we observed an asymptotic mechanical response prior to yielding, similar to plastic deformation in metals (Fig. 2b). The stress–strain curve in Fig. 2b supports the notion of connected fillers, whereby the networks break as strain is increased, leading to the flattening of the stress–strain curve at higher strains. This phenomenon is further investigated by varying the volume of filler (Fig. 2d). When ϕ = 30%, the pre-compressed ST3R and solid FM samples gave comparable modulus (12–15 MPa). At ϕ = 50%, however, a dramatic change in modulus is observed in the ST3R (Fig. 2d). This is consistent with the formation of networks whereby a minimum filler volume is required.

Since solidification is a stochastic (thermodynamic phase transformation) process, it is expected that strain-driven changes in the modulus will lead to significant differences between ST3R and analogous composites where no phase change occurs. The change in elasticity should, therefore, manifest as an asymmetry in the distribution of complex stiffness leading to a unique trend in skewness for the ST3R composite under dynamic stress compared to static (non-responsive) analogous composites (*e.g.* EGaIn, solid FM or glycerol). To confirm this inference, we performed dynamic tensile strain on thin rectangular samples (1.0 × 0.5 × 0.1 cm) at 1 Hz, with increasing amplitudes from 5–15% strain. As expected, ST3R composite shows an increase in complex stiffness as strain is increased (Fig. 2e), supporting the notion of a strain hardening material. We infer that the rise in complex stiffness is a result of partial solidification of the undercooled liquid metal, induced by deformation of the composite. In contrast, EGaIn fillers show a small initial rise in normalized complex stiffness before a decrease as strain is increased. Additional control experiments of solid FM particles, glycerol droplets, and PDMS (matrix) further show a decrease in stiffness as strain is increased, highlighting the unique behavior of the ST3R (Fig. 2e). We also observed a shift in skewness of the distribution of complex stiffness (Fig. 2f), whereby positive values represent bias in the mass of the distribution towards lower stiffness and negative values point towards higher stiffness. It is therefore evident that only the ST3R composite displayed a shift towards higher complex stiffness. Although stiffness is enhanced after mechanical loading, the increase is on the order of 10%. Analysis of the stressed composite samples (DSC) indicates that under these experimental conditions, only 14% of undercooled particles solidified after tensile elongation (Fig. S3, ESI†) while total solidification was obtained with the compressed samples. This low conversion correlates with modest increase in stiffness, which highlights that stiffness transformation is limited in tension and will not occur under small perturbations. Thus, special handling of the composite is not required under our experimental conditions.

To further explore the effect of compression on metastable particle transformation, we performed a series of experiments by varying compressive stress on ϕ = 50% samples. Young's modulus increases with the compressive stress up to 33 MPa (Fig. 3a). Although 68% strain was produced, more than half springs back, which resulted in approximately 30% permanent deformation (Fig. S4 and S5, ESI†). Further increment to 70 MPa leads to a decrease in Young's modulus, which is attributed to damage to the composite as suggested by the transition to higher compressive stiffness due to solid dominated deformation (Fig. S5, ESI†).

Complete solidification was observed even under low compression load irrespective of ϕ (Fig. 3b and c). This indicates that the continuous rise in Young's modulus (at low compressions) has a structural component in addition to the solidification of the metal, which could originate from changes in volume, shape or texture of the solidified metal and the formation of an interconnected network. Further evidence of total solidification is provided from scanning electron microscopy (SEM). Evaluating differences in particle shape by SEM before and after compression shows uniform spherical

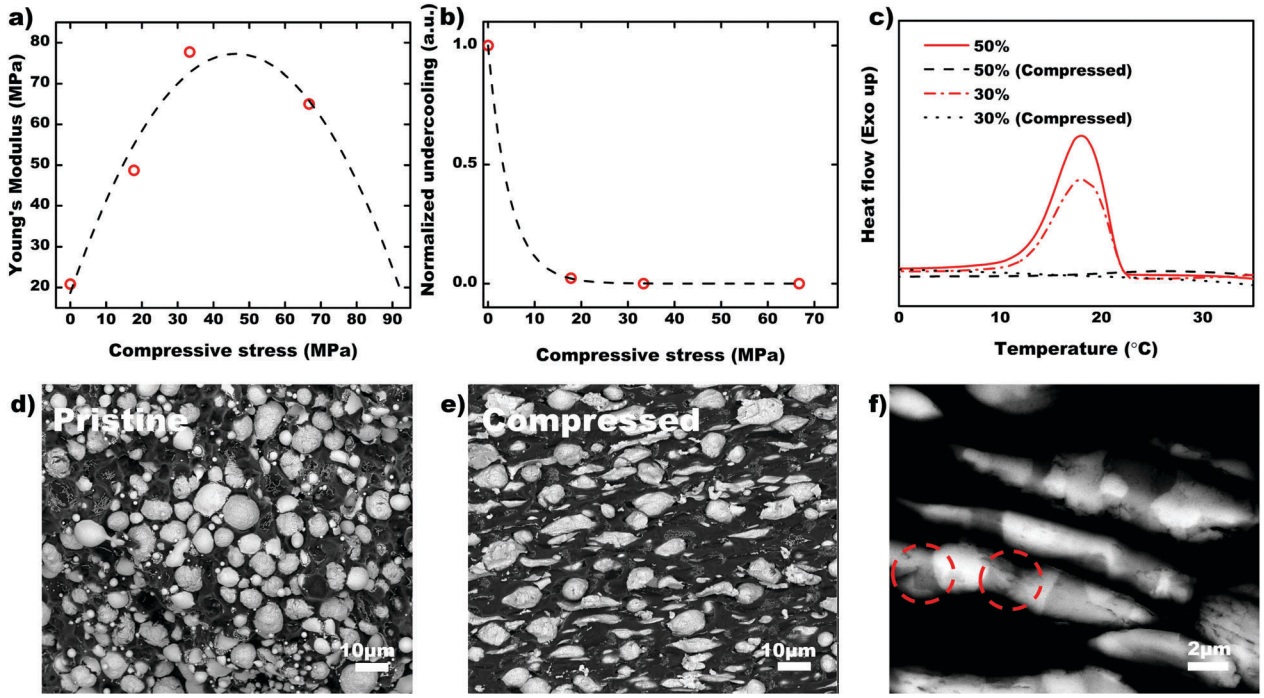

Fig. 3 (a) Young's modulus as a function of increasing compression stress for ϕ = 50% samples. Line represents a guide to the eye. (b) Normalized fraction of undercooling for ϕ = 50% ST3R composites. (c) Cooling curve from differential scanning calorimetry (DSC) of pristine and compressed (33 MPa) ST3R composite. (d and e) Scanning electron micrographs (SEM) of pristine and compressed ϕ = 50% undercooled FM composite in backscattered mode. (f) Magnified micrograph showing *Z* contrast within the field's metal after compression due to spinodal decomposition. The insert highlights point of fusion between different particles with these interconnects being stochastically distributed throughout the material.

particles in the uncompressed sample (Fig. 3d) while oblong/elongated particles are observed in the compressed samples (Fig. 3e). Solid FM composite in contrast, showed negligible changes in particle appearance (Fig. S6, ESI†). Solidification of metallic alloys occurs with concomitant spinodal decomposition and hence changes in sub-surface composition. Analyzing contrast in the fillers with SEM using an energy selective backscattered (EsB) detector shows uniform contrast in the uncompressed sample (Fig. S7, ESI†). Upon compression, however, spinodal decomposition is observed (Fig. 3f) on the metallic phase *via* *Z*-contrast of backscattered electrons and differences in elemental composition is confirmed (Fig. S8, ESI†) using energy dispersive X-ray spectroscopy (EDS).

Reconfigurable deformation. As observed in the compressed samples, permanent deformation due to modulus changes can be achieved by stressing the material. Fig. 4a and b illustrates that the shape of ST3R composite is tunable, in this case by twisting a straight sample. The initially compliant liquid fillers allow the composite shape to be easily reconfigured. Deformation and reshaping, with concomitant solidification, of the metal filler locks the composite in the new configuration. The resultant shape is dictated by the distribution of applied stress field. The strip retains its new shape after the applied stress is removed (Fig. 4b).

Furthermore, controlled indentation with a blunt object can lead to wells of tunable depth (see profilometry of an example, insert Fig. 4c). A linear correlation between applied force and depth of the wells (Fig. S9, ESI†) shows that the compressive deformation is highly tunable with the uniformity of indented regions with increasing compressive stress (Fig. S9 inset, ESI†). An example of wells holding a liquid while the undeformed

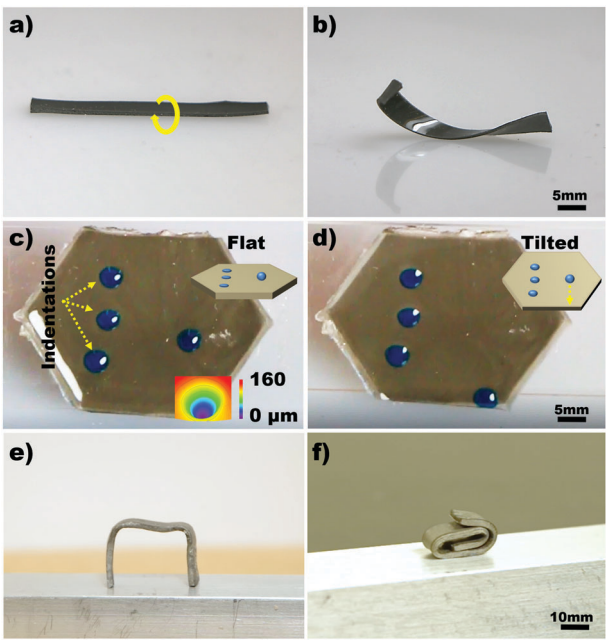

Fig. 4 (a and b) Twist deformation leading to swirled composite. (c and d) Wells formed by selective compression. (e and f) Reconfiguration of the composite by melting and re-solidifying into a new shape.

portion releases the liquid when tilted, is demonstrated in Fig. 4c and d. A combination of shaping by twisting/bending and compression can also lead to changes in surface topology as illustrated with a slanting strip that can also hold water (Fig. S10, ESI†).

Since the deformed shape is due to solidification, it can readily be reconfigured by an inverse phase transformation (melting) as previously shown.[21,22,43,47] We demonstrate that the first solidification from metastable liquid to solid, ST3R transitions into a typical metal–elastomer composite (state 2, Fig. 1f), whereby its shape can be reconfigured or changed by melting the metal filler (ESI,† Fig. S11). Under such circumstances, the elastomer is locked in place when the metal solidifies as shown in Fig. 4e and f. During the melting process, the composite can be observed to relax and partially retain its original shape due to the elastic response from the matrix (Fig. S11, ESI†).

Conclusions

We have developed a mechanically triggered stiffness tunable composite material by managing the interplay between thermodynamic relaxation and response of metastable liquid metal to mechanical (tensile or compressive) stress. Stiffness change can be selectively targeted resulting in the ability to couple material transformation with shape reconfiguration. Composites with such capabilities could find unique applications as mechanically adaptive or responsive (smart) materials where external sources of energy such as heat or electricity are not available. Furthermore, as the metastable particles do not rely on a specific material chemistry, self-stiffening behaviour can be incorporated into diverse materials and applications ranging from sensors and functional devices to reconfigurable structures and robotics.

Experimental

Materials

Eutectic indium (51%)–bismuth (32.5%)–tin (16.5%) (field's metal) was purchased from Rotometals. Eutectic gallium (75.5%)–indium (24.5%) was purchased from Sigma Aldrich. Slygard 184 was purchased from Ellsworth adhesives. Ethanol (>99.2%) was purchased from Decon Laboratories Inc. Glacial acetic acid (99.7%) was purchased from Fisher scientific. Diethylene glycol (99.9%) was purchased from VWR.

Methods

Preparing liquid metal core shell particles. The SLICE (shearing liquids into complex particles) method was applied to produce all the particles used in this work. In a typical synthesis, 2.5 g of field's metal was placed into a vial containing 5 ml of solvent (diethylene glycol containing 5% acetic acid). The vial was then heated using an oil bath at 145 °C. After 5 minutes, a teflon stirrer attached to a Dremel tool is placed into the vial, making sure that contact is made with the molten metal. The solution is stirred with gradual increase from 0–22 000 rpm. The shearing was maintained at this speed for 10 minutes, and the vial is subsequently removed from the oil bath with continuous shearing. Once the vial is completely out of the oil bath, the speed of the Dremel tool is gradually reduced back down to 0 rpm. The resulting grey solution is then filtered and rinsed using ethanol to remove residual solvent. Based on inspection by SEM, particle size ranged from 1–20 μm.

Preparing composite. As a general procedure, core shell particles of desired amount were first filtered and dried on filter paper, and then added onto premixed (10 : 1 ratio) Sylgard 184. In a typical preparation, 8 g of field's metal undercooled particles are added into 1 g of Sylgard 184. The mixture is stirred for at least 10 minutes until a homogeneous mixture is achieved before outgassing. During this process, it is expected that some undercooled particles might be triggered and solidify, however, based on DSC and mechanical data a majority are not affected. The same procedure is used for all other fillers. Curing was performed at 100 °C for approximately 12 hours in a glass mold (4.0 × 4.0 × 0.1 cm) sprayed with mold release (Mann®). The composite was subsequently cut into 4 × 0.5 × 0.1 cm rectangular strips using a razor. Composites for dynamic mechanical testing were molded in polystyrene weigh boats, thus, these samples were cured at 60 °C. These samples were cut into 2.0 × 0.5 × 0.1 cm using a razor.

Differential scanning calorimetry (DSC) was performed using TA Instruments Q2000 (heating/cooling rate = 10 °C min^{-1}). For example, 3 mg of particles are added into an aluminium pan, and subsequently placed into the DSC stage, which has a temperature of 40 °C by default. The temperature is held constant for 5 minutes to achieve equilibrium before performing cooling/heating.

Scanning electron microscopy (SEM) of the undercooled particles in Fig. 1a were obtained using JEOL JSM-6060LV with a secondary electron detector (ET detector) and accelerating voltage of 20 kV. Micrographs of the composite were taken using an FEI Inspect F50 with a backscattered electron detector to obtain contrast between the matrix and fillers. Accelerating voltage was initially set to 8 kV but to further increase Z contrast (to show spinodal decomposition), it was increased to 30 kV.

Mechanical testing. Dynamic mechanical analysis (DMA) measurements in tension mode were performed using TA Instruments Q800. Dynamic strain was set at 1 Hz and static force at 0.01 N with increasing amplitude from 500 μm to 1600 μm. Tension tests were performed on Instron 5944 single column testing system using pneumatic grips and an extension rate of 1 mm s^{-1}. The initial gauge length is maintained at 27 mm for both pristine and pre-compressed samples.

Conflicts of interest

There are no conflicts of interest to declare.

Acknowledgements

This work was supported by Iowa State University through startup funds to M. M. T. and M. D. B. M. M. T was also

supported through a Black and Veatch faculty fellowship. SO-R was supported in part by a GMAP fellowship from Iowa State University. The authors would also like to thank Chad Macziewski for technical assistance.

References

1 F. J. McGarry, *Annu. Rev. Mater. Sci.*, 1994, **24**, 63–82.
2 H. Meng and G. Li, *Polymer*, 2013, **54**, 2199–2221.
3 G. B. Hadjichristov, Y. G. Marinov, A. G. Petrov, E. Bruno, L. Marino and N. Scaramuzza, *J. Appl. Phys.*, 2014, **115**, 083107/083101.
4 X.-F. Wu and A. L. Yarin, *J. Appl. Polym. Sci.*, 2013, **130**, 2225–2237.
5 N. D. Wanasekara, D. A. Stone, G. E. Wnek and L. T. J. Korley, *Macromolecules*, 2012, **45**, 9092–9099.
6 L. E. Strong and J. L. West, *Wiley Interdiscip. Rev.: Nanomed. Nanobiotechnol.*, 2011, **3**, 307–317.
7 H. Kim and S. Kwon, *Science*, 2013, **339**, 150–151.
8 M. T. Byrne and Y. K. Gun'ko, *Adv. Mater.*, 2010, **22**, 1672–1688.
9 T. Sun and G. Qing, *Adv. Mater.*, 2011, **23**, H57–77.
10 J. Benson, I. Kovalenko, S. Boukhalfa, D. Lashmore, M. Sanghadasa and G. Yushin, *Adv. Mater.*, 2013, **25**, 6625–6632.
11 J. Jeon, H.-B.-R. Lee and Z. Bao, *Adv. Mater.*, 2013, **25**, 850–855.
12 D. Ge, E. Lee, L. Yang, Y. Cho, M. Li, D. S. Gianola and S. Yang, *Adv. Mater.*, 2015, **27**, 2489–2495.
13 S. Yao and Y. Zhu, *Adv. Mater.*, 2015, **27**, 1480–1511.
14 J. Di, X. Zhang, Z. Yong, Y. Zhang, D. Li, R. Li and Q. Li, *Adv. Mater.*, 2016, **28**, 10529–10538.
15 M. D. Bartlett, A. Fassler, N. Kazem, E. J. Markvicka, P. Mandal and C. Majidi, *Adv. Mater.*, 2016, **28**, 3726–3731.
16 S. H. Jeong, S. Chen, J. Huo, E. K. Gamstedt, J. Liu, S.-L. Zhang, Z.-B. Zhang, K. Hjort and Z. Wu, *Sci. Rep.*, 2015, **5**, 18257.
17 M. D. Bartlett, N. Kazem, M. J. Powell-Palm, X. Huang, W. Sun, J. A. Malen and C. Majidi, *Proc. Natl. Acad. Sci. U. S. A.*, 2017, **114**, 2143–2148.
18 F. Ilievski, A. D. Mazzeo, R. F. Shepherd, X. Chen and G. M. Whitesides, *Angew. Chem., Int. Ed.*, 2011, **50**, 1890–1895.
19 D. Rus and M. T. Tolley, *Nature*, 2015, **521**, 467–475.
20 R. F. Shepherd, F. Ilievski, W. Choi, S. A. Morin, A. A. Stokes, A. D. Mazzeo, X. Chen, M. Wang and G. M. Whitesides, *Proc. Natl. Acad. Sci. U. S. A.*, 2011, **108**, 20400–20403.
21 I. M. Van Meerbeek, B. C. MacMurray, J. W. Kim, S. S. Robinson, P. X. Zou, M. N. Silberstein and R. F. Shepherd, *Adv. Mater.*, 2016, **28**, 2801–2806.
22 A. Tonazzini, S. Mintchev, B. Schubert, B. Mazzolai, J. Shintake and D. Floreano, *Adv. Mater.*, 2016, **28**, 10142–10148.
23 Q. Zhang, K. Zhang and G. Hu, *Sci. Rep.*, 2016, **6**, 22431.
24 W. Wang, H. Rodrigue and S.-H. Ahn, *Sci. Rep.*, 2016, **6**, 20869.
25 K. C. Hribar, R. B. Metter, J. L. Ifkovits, T. Troxler and J. A. Burdick, *Small*, 2009, **5**, 1830–1834.
26 M. Wang, H. Singh, T. A. Hatton and G. C. Rutledge, *Polymer*, 2004, **45**, 5505–5514.
27 V. Q. Nguyen, A. S. Ahmed and R. V. Ramanujan, *Adv. Mater.*, 2012, **24**, 4041–4054.
28 V. Ramachandran, M. D. Bartlett, J. Wissman and C. Majidi, *Extreme Mech. Lett.*, 2016, **9**, 282–290.
29 C. Tridech, H. A. Maples, P. Robinson and A. Bismarck, *ACS Appl. Mater. Interfaces*, 2013, **5**, 9111–9119.
30 H. A. Maples, S. Wakefield, P. Robinson and A. Bismarck, *Compos. Sci. Technol.*, 2014, **105**, 134–143.
31 S. Daynes, K. Potter and P. Weaver, *Compos. Sci. Technol.*, 2008, **68**, 3431–3437.
32 B. Wang and K. S. Fancey, *Mater. Lett.*, 2015, **158**, 108–110.
33 S. R. White, N. R. Sottos, P. H. Geubelle, J. S. Moore, M. R. Kessler, S. R. Sriram, E. N. Brown and S. Viswanathan, *Nature*, 2001, **409**, 794–797.
34 K. S. Toohey, N. R. Sottos, J. A. Lewis, J. S. Moore and S. R. White, *Nat. Mater.*, 2007, **6**, 581–585.
35 Z. S. Kean and S. L. Craig, *Polymer*, 2012, **53**, 1035–1048.
36 A. L. B. Ramirez, Z. S. Kean, J. A. Orlicki, M. Champhekar, S. M. Elsakr, W. E. Krause and S. L. Craig, *Nat. Chem.*, 2013, **5**, 757–761.
37 Q. Wang, G. R. Gossweiler, S. L. Craig and X. Zhao, *J. Mech. Phys. Solids*, 2015, **82**, 320–344.
38 H. M. Klukovich, Z. S. Kean, S. T. Iacono and S. L. Craig, *J. Am. Chem. Soc.*, 2011, **133**, 17882–17888.
39 A. L. Black, J. A. Orlicki and S. L. Craig, *J. Mater. Chem.*, 2011, **21**, 8460–8465.
40 G. R. Gossweiler, G. B. Hewage, G. Soriano, Q. Wang, G. W. Welshofer, X. Zhao and S. L. Craig, *ACS Macro Lett.*, 2014, **3**, 216–219.
41 T. Chung, A. Romo-Uribe and P. T. Mather, *Macromolecules*, 2008, **41**, 184–192.
42 X. Luo and P. T. Mather, *ACS Macro Lett.*, 2013, **2**, 152–156.
43 Q. Ge, A. Serjouei, H. J. Qi and M. L. Dunn, *Int. J. Solids Struct.*, 2016, **102-103**, 186–199.
44 Y. Xi, D. Chai, W. Zhang and J. Zhou, *Scr. Mater.*, 2006, **54**, 19–23.
45 V. Recarte, R. Pérez-Sáez, E. Bocanegra, M. Nó and J. San Juan, *Mater. Sci. Eng., A*, 1999, **273**, 380–384.
46 S. Cinar, I. D. Tevis, J. Chen and M. Thuo, *Sci. Rep.*, 2016, **6**, 21864.
47 W. Shan, T. Lu and C. Majidi, *Smart Mater. Struct.*, 2013, **22**, 085008.
48 I. D. Tevis, L. B. Newcomb and M. Thuo, *Langmuir*, 2014, **30**, 14308–14313.
49 L. Cademartiri, M. M. Thuo, C. A. Nijhuis, W. F. Reus, S. Tricard, J. R. Barber, R. N. Sodhi, P. Brodersen, C. Kim and R. C. Chiechi, *J. Phys. Chem. C*, 2012, **116**, 10848–10860.

